Clim Dyn (2018) 50:1353–1371
DOI 10.1007/s00382-017-3689-7

Westerly wind bursts simulated in CAM4 and CCSM4

Tao Lian[1] · Youmin Tang[1,2] · Lei Zhou[1,3,4] · Siraj Ul Islam[2] · Chan Zhang[1] · Xiaojing Li[1] · Zheng Ling[5]

Received: 12 October 2016 / Accepted: 11 April 2017 / Published online: 20 April 2017

Abstract The equatorial westerly wind bursts (WWBs) play an important role in modulating and predicting the El Niño-Southern Oscillation (ENSO). In this study, the ability of the Community Atmospheric Model version 4 (CAM4) and the Community Climate System Model version 4 (CCSM4) in simulating WWBs is systematically evaluated. Many characteristics of WWBs, including their longitude distributions, durations, zonal extensions, variabilities at seasonal, intraseasonal, and interannual timescales, as well as their relations with the Madden–Julian Oscillation (MJO) and ENSO, are discussed. Generally speaking, these characteristics of WWBs can be successfully reproduced by CAM4, owning to the improvement of the deep convection in the model. In CCSM4, significant bias such as the lack of the equatorial Pacific WWBs in boreal spring season and the weak modulation by a strong MJO are found. Our findings confirm the fact that the WWBs are greatly modulated by the surface temperature. It's also suggested that improving the air-sea coupling in CCSM4 may improve model performance in simulating WWBs, and may further improve the predictability of ENSO in the coupled model.

✉ Tao Lian
liantao@sio.org.cn

[1] State Key Lab of Satellite Ocean Environment Dynamics, Second Institute of Oceanography, Hangzhou, China

[2] Environmental Science and Engineering, University of Northern British Columbia, Prince George, Canada

[3] Institute of Oceanography, Shanghai Jiao Tong University, 800 Dongchuan Road, Shanghai 200240, China

[4] Laboratory for Regional Oceanography and Numerical Modeling, Qingdao National Laboratory for Marine Science and Technology, Qingdao 266061, China

[5] Guangdong Key Laboratory of Coastal Ocean Variability and Disaster Prediction, Guangdong Ocean University, Zhanjiang, China

1 Introduction

Westerly wind bursts (WWBs), the sudden but strong westerly zonal wind anomalies, are a distinct synoptic to intraseasonal atmospheric feature in the tropics from the Indian Ocean to the central Pacific Ocean (Hartten 1996; Harrison and Vecchi 1997; Seiki and Takayabu 2007). WWBs play an important role in the tropical climate (see the review in Lengaigne et al. 2004). In particular, WWBs over the western and central equatorial Pacific can drive strong anomalous eastward sea surface currents that lead to the increase in the sea surface temperature (SST) in the central equatorial Pacific, and induce downwelling Kelvin waves within the equatorial wave guide which is crucial to the warm SST anomalies in the eastern tropical Pacific (McPhaden et al. 1988; Lengaigne et al. 2002, 2003). Thus, WWBs are regarded as a fundamental process for modulating the El Niño-Southern Oscillation (ENSO; McPhaden 1999; Vecchi and Harrison 2000). Recent studies further indicate that WWBs are also a source of the diversity and asymmetry of ENSO (Lian et al. 2014; Fedorov et al. 2014; Hu et al. 2014; Chen et al. 2015).

Simulating WWBs in a model is therefore important for the ENSO simulation and forecast (McPhaden et al. 2015). It has been reported that several atmospheric general circulation models (AGCMs) can simulate WWBs (Liess et al. 2004; Vecchi et al. 2006; Miyama and Hasegawa 2014). However, it's still not clear whether the Community Atmospheric Model (CAM), one of the popular AGCMs, can simulate WWBs. Using the Interactive Ensemble technique (Kirtman et al. 2009), Lopez et al. (2013) found

that most atmospheric noise activities in CAM version3 (CAM3; Collin et al. 2006) were weak and occurred outside the domain of the observed WWBs. As a result, a parameterization scheme designed for intermediate models (Gebbie et al. 2007; Gebbie and Tziperman 2009) had to be added in the Community Climate System Model version 3 (CCSM3), of which CAM3 is the atmospheric component, so that the role of WWBs on ENSO could be studied. This technique was also used in CCSM4, when the atmospheric component evolved to CAM version4 (CAM4; Gent et al. 2011; Neale et al. 2013), to explore the role of WWBs in ENSO (Lopez et al. 2013). On the other hand, Neale et al. (2008) indicated there was a series of WWBs proceeding El Niño in CCSM3. Subramanian et al. (2011) showed that the Madden–Julian Oscillation (MJO; Madden and Julian 1971) simulation in CAM4 was greatly improved. Because MJO and WWBs are closely related to some extent (Puy et al. 2015), the simulation of WWBs in CAM4 is also expected to be improved. Recently, Hu and Fedorov (2016) presented that the CESM, the new version of CCSM4, could generate its own WWBs occasionally, and these WWBs were important for El Niño development. Whether the CAM4 and CCSM4 can simulate WWBs should be clarified.

Using 18 climate models in the Coupled Model Intercomparison Project phase 3 (CMIP3), Seiki et al. (2011) assessed the simulation of WWBs and its relation with ENSO. They found that the robust dependence of WWBs on ENSO is reproduced by some coupled models. However, some other fundamental characteristics of WWBs were not fully explored. For example, it's not clear whether the modeled WWBs exhibit a stronger phase locking characteristic in boreal winter when more WWBs occur (Harrison and Vecchi 1997). It has not be examined yet whether the WWBs in late boreal spring and summer seasons over the central equatorial Pacific, which is important for triggering and maintaining the strong El Niño (McPhaden 1999; Menkes et al. 2014; Chen et al. 2015; Xue and Kumar 2016; Hu and Fedorov 2016; Lian et al. 2017), can be correctly simulated in the coupled model. It's also not clear whether the spatial pattern of WWBs is realistically reproduced in the state-of-the-art models. The relation between MJO and WWBs in the coupled model is also less discussed before.

In this study, we systematically assess the ability of CAM4 and CCSM4 in representing WWBs and explore possible mechanisms of WWBs in the models. The rest of the paper is arranged as follows. The model and data are introduced in Sect. 2. The features of the simulated WWBs in CAM4, including their longitude distributions, durations, zonal extensions, variabilities at seasonal, intraseasonal and interannual timescales, as well as their relations with MJO and ENSO, are shown in Sect. 3. In Sect. 4, we evaluate the performance of CCSM4 in simulating WWBs. The origin of WWBs simulated in models is explored in Sect. 5, followed by the conclusions and discussion in Sect. 6.

2 Model and data

CAM4 is the seventh AGCM developed by the National Center for Atmospheric Research (NCAR). Compared with CAM3, the mean state and the variability of the atmospheric climate, in particular the representation of the MJO, are significantly improved (Subramanian et al. 2011; Zhou et al. 2012; Neale et al. 2013). The details of CAM4 configuration and performance can be found in Gent et al. (2011) and in Neale et al. (2013). In this study, the atmosphere-only experiments are conducted using CAM4, which has 26 vertical levels from the earth surface (about 992.5 hPa) to the top of the stratosphere (about 3.5 hPa) and a horizontal resolution of 2.5° longitude × 1.875° latitude. The model is forced by the merged daily SST/land Skin temperature from the comprehensive ocean–atmosphere data set (CODAS). This is also the boundary condition used in the National Centers for Environmental Prediction/National Center for Atmospheric Research (NCEP/NCAR) reanalysis (Kalnay et al. 1996). Five model ensemble runs with different initial conditions are conducted for 60 years from 1948 to 2007, labeled as CAM4#1 to CAM4#5 hereafter. The coupled model experiments are conducted with CCSM4, which includes the atmosphere, ocean, land, and sea ice components. The atmospheric component of CCSM4 is CAM4, which remains the same configurations as they are in the atmosphere-only ones. The oceanic component is the Parallel Ocean Program version 2 (POP2; Smith et al. 2010). The resolution of POP2 is roughly 1.0° longitude × 0.5° latitude and gradually increases to 0.27° latitude near the equator. There are 60 vertical levels in POP2. The land component is the Community Land Model version 3.5 (Oleson et al. 2008) and the sea ice component is the Community Ice Code version 4 (Hunke and Lipscomb 2008). More details of CCSM4 configuration and performance can be found in Gent et al. (2011). In this study, the CCSM4 is integrated for 150 years, and the results from the last 50 years are used for analysis.

Daily winds at 10 m and the upward longwave radiation flux at the top of atmosphere from NCEP/NCAR reanalysis are used for the verification of model simulations. The latter is used to represent the outgoing longwave radiation (OLR) in the present study. The horizontal resolution of the NCEP/NCAR reanalysis is 2.5° longitude × 2.5° latitude. The anomaly in the following analysis is defined as the departure from the 60-year annual mean.

For both observations and model simulations, a WWB should satisfy (1) the surface zonal westerly anomaly averaged between 5°S and 5°N exceeds 5.0 m s^{-1}; (2) the zonal

extension of the area satisfying (1) should be at least 10° in longitude; (3) the above 2 conditions last for at least 2 days. Note that the above criterion of exceeding 5.0 m s^{-1} is based on the variance in the zonal wind anomalies. In CAM4 and CCSM4, the standard deviations of zonal winds are very close to that in observations (not shown). Therefore, we can use the same WWBs criterion for observations, CAM4, and CCSM4. In order to scale the integral effect of the zonal wind anomalies related to a WWB over a given region, a "WWB measure" index is defined as the mean zonal surface wind anomalies over an interested region related to WWBs (Chen et al. 2015). The multivariate index created in Wheeler and Hendon (2004) is used to represent the MJO. The Niño3.4 index, representing ENSO, is defined as the mean SST within 170°W–120°W and 5°S–5°N. In both observations and models, the El Niño (La Niña) years are defined as the years when the Niño 3.4 index in the DJF season is greater (smaller) than one positive (negative) standard deviation.

3 WWBs simulations in CAM4

3.1 General features

Since the definition of the WWBs depends on the mean state of the surface zonal wind, the climatological surface winds in CAM4 are compared with the observations. The observed surface wind in the global tropical band is well represented in CAM4 (Fig. 1a, b). The magnitudes of the surface zonal winds are moderately overestimated in the southern Indian Ocean, off the equatorial Pacific and the equatorial Atlantic, while they are slightly underestimated in the northern Indian Ocean (Fig. 1c). In the equatorial Indo-Pacific region where the WWBs occur, the model bias in zonal winds is very small. The maximum bias is found over the western Indian Ocean with a value less than 1.0 m s^{-1}.

Figure 2a gives the longitudinal distribution of WWBs over the equatorial region in observations. WWBs are distributed over two longitudinal regions, from 40°E to 100°E and from 130°E to 160°W, although a few WWBs are observed out of these 2 regions (Seiki and Takayabu 2007). Thus, the study domains in this study are the equatorial Indian Ocean (IO; 40E°–100°E, 5°S–5°N), the western Pacific (WP; 130°–160°E, 5°S–5°N), and the central Pacific (CP; 160°E–160°W, 5°S–5°N). Two regions are marked in the equatorial Pacific because the relations between ENSO and WWBs in the WP and CP regions are different, as will be shown in the following sections. The numbers of WWBs over the IO, WP, and CP regions are 342, 233 and 191 for 60 years, with an average of 5.70, 3.88, and 3.18 per year, respectively. The number of WWBs found here seems smaller than those reported in previous studies (Harrison and Vecchi 2000; Harrison and Chiodi 2009). But actually, as summarized in Puy et al. (2015), such discrepancy is mainly due to different definitions of WWBs.

The longitudinal distribution of WWB occurrence over the equatorial band in CAM4 is comparable with observations, as shown in Fig. 2b. WWBs are mainly found over

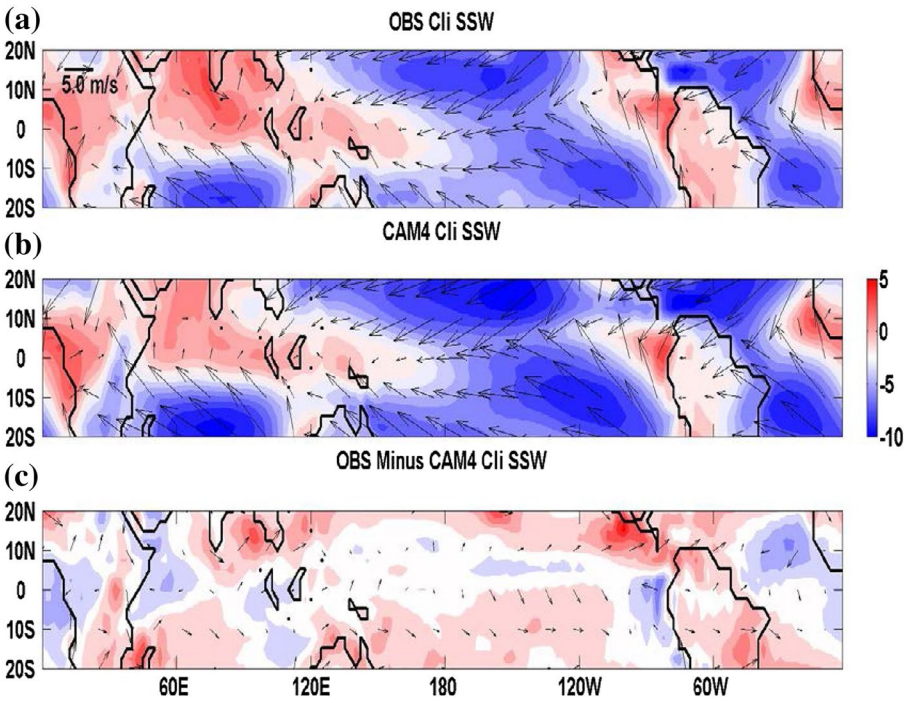

Fig. 1 Climatological surface winds (vector, unit of m s^{-1}) and the zonal surface winds (*color*, unit of ms^{-1}) in observations (**a**), CAM4 (**b**), and their differences (**c**)

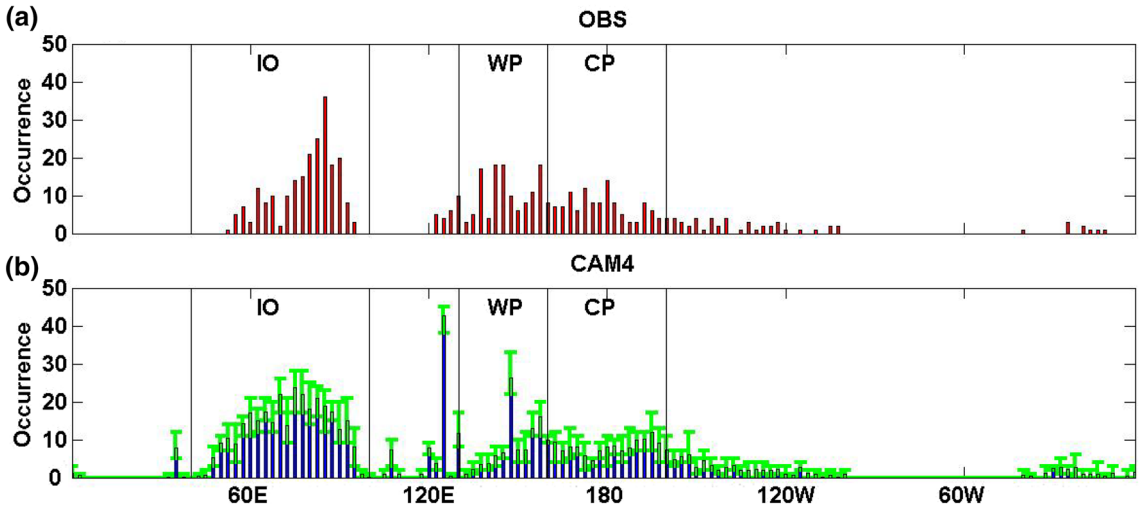

Fig. 2 Longitudinal distribution of the integrated WWB occurrence in observations (**a**) and CAM4 (**b**). *Green bars* in **b** show the ranges of ensemble spreads

the IO, WP, and CP regions. A lot of simulated WWBs unexpectedly exist at 124°E, probably due to the model bias in simulating surface wind toward the New Guinea. The average numbers of WWBs in the 5 ensembles over the IO, WP and CP regions are 306, 104 and 132, with an average of 5.10, 1.73, and 2.20 per year, respectively. The number of WWBs is underestimated in CAM4, especially in the equatorial Pacific region.

Figure 3 compares the histograms of the duration and the zonal extension of the WWBs in observations and model simulations, respectively. In Fig. 3a–c, the window of each bin is 5 days, thus the actual duration of WWBs is the central value of a bin ±2.5 days, for example, the bin centered around 10 days includes the WWBs with a duration from 7.5 to 12.5 days. Similarly, in Fig. 3d–f, longitudes of 10° are designed as the window, so that, for example, the 20° bin includes the WWBs with a zonal extension from 15° to 25° in longitude. In general, there is a peak of WWB occurrence around the duration of 15 days, and a peak of WWB's zonal extension around 20° in both observations and model simulations. In all 3 regions, the majority of the observed and simulated WWBs, roughly 60%, have a duration less

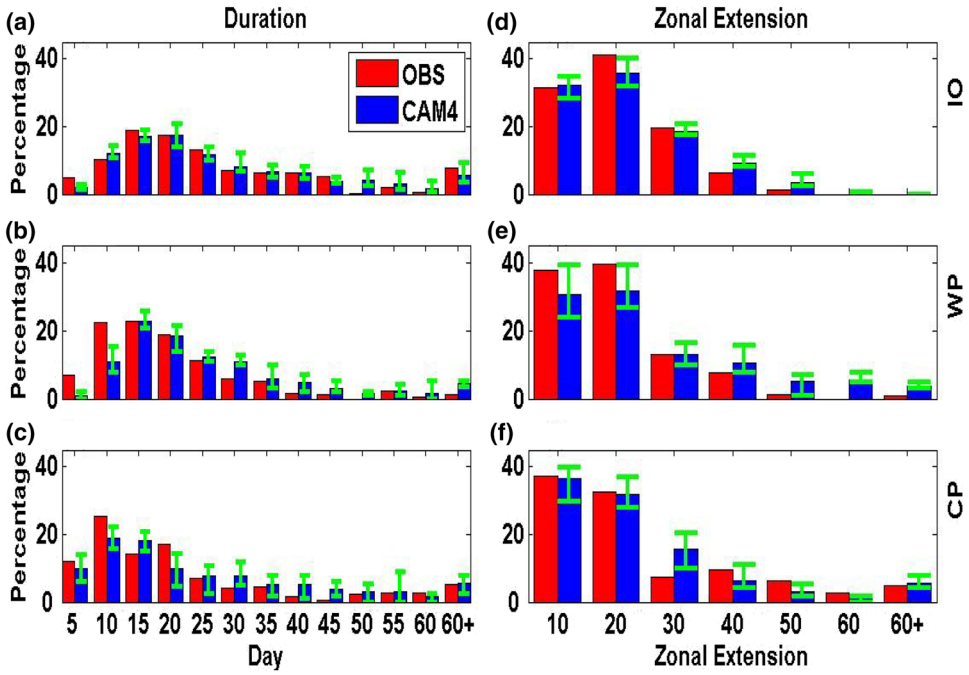

Fig. 3 The percentage of WWBs found in IO (*upper row*), WP (*middle* row) and CP (*lower row*) as a function of the duration (*left panel*) and the zonal extension (*right panel*). *Red* and *blue bars* denote the percentage of the WWBs occurring with respect to the total WWBs numbers in observations and CAM4, respectively. *Green bars* show the ranges of ensemble spreads

than 35 days. The zonal extension of most observed and simulated WWBs is less than 30°, although there are more simulated WWBs over the IO and WP regions with a zonal extension larger than 30°. Despite these discrepancies, the short duration and the limited zonal extension of the observed WWBs are captured by the model.

3.2 Seasonal and interannual variabilities of WWBs

Figure 4a–c compares the monthly distribution of the observed and simulated WWB occurrence in the three regions. Over the IO region, two peaks of observed WWB occurrence are found around June and December (Fig. 4a). CAM4 correctly captures these two peaks, although more WWBs are simulated in boreal winter. Over the WP and CP regions, more WWBs are observed in boreal winter (Fig. 4b, c), which is consistent with Harrison and Vecchi (1997). There is a weak peak around April in the WP region. Recent studies suggest that WWBs in the WP occurring in later spring and boreal summer play an important role in maintaining the El Niño (McPhaden 1999; Menkes et al. 2014; Chen et al. 2015; Xue and Kumar 2016; Lian et al. 2017). It's clear that CAM4 successfully captures the seasonality of the WWB occurrence over these two regions. However, the WWB occurrence in CAM4 does not show distinct peaks over the WP and CP regions. Note that the temporal peak of a WWB is used to denote when this WWB occurs. As a result, a bias in simulating when a WWB reaches the peak can lead to bias in the simulated seasonality of WWB occurrence. On the other hand, each WWB can last for several days. If looking at the monthly distribution of the number of days with WWBs, the simulated seasonality is greatly improved in the WP and CP regions (Fig. 4e, f). Our results indicate that CAM4 has a good performance in simulating the monthly distribution of WWBs, but there is a significant bias in simulating the seasonality of the temporal peak of WWBs in the WP and CP regions.

The histograms of the WWB measure are given in Fig. 4g–i, showing comparable seasonal variabilities, with a large WWB measure during the IO monsoon transition period over the IO (Fig. 4g) and during boreal winter over the WP/CP regions (Fig. 4h, i). It is clear that there is a large model bias for the annual cycle of WWB measure over the IO region. However, over the WP and CP regions, the WWB measure's seasonality is well captured. Since the WWB measure denotes the integral effect of WWBs, via wind stress, on the underlying surface, a better reproduction

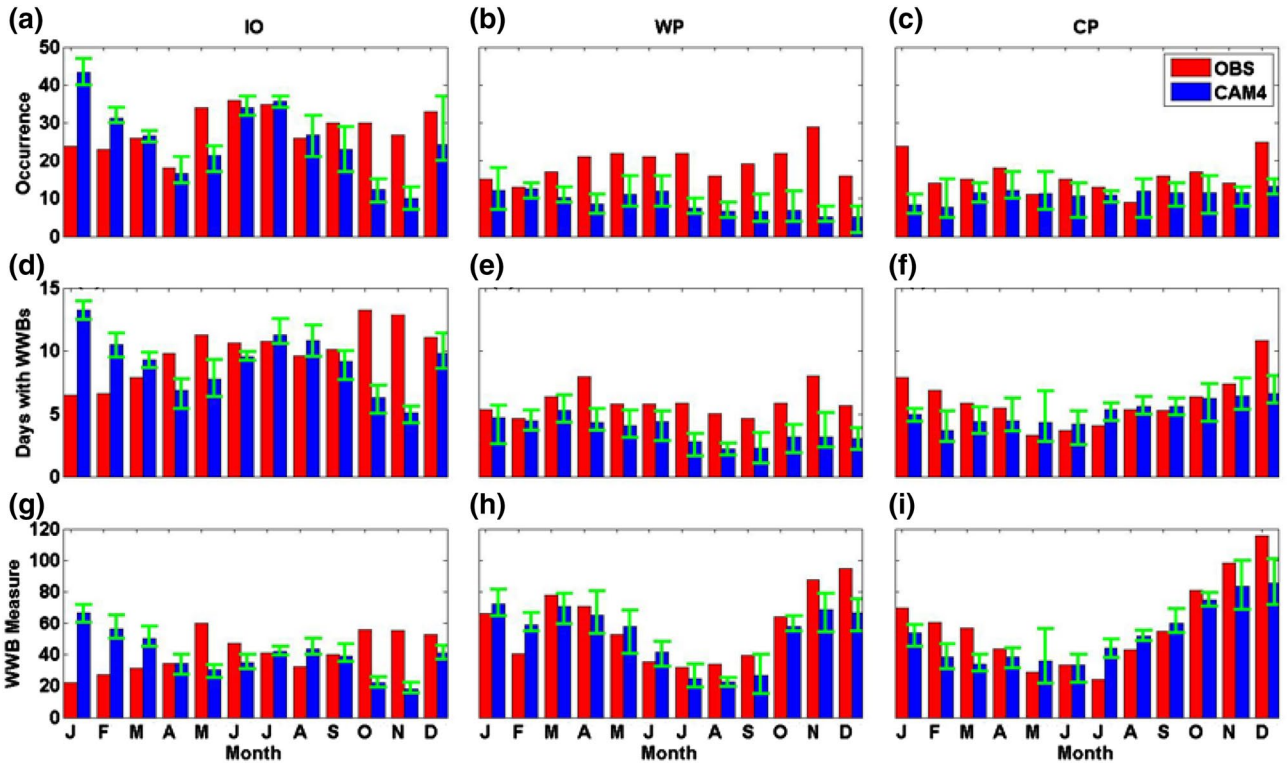

Fig. 4 Monthly distribution of the occurrence (*upper row*), number of days with WWBs (*middle row*), and WWB measure (*lower row*, unit of 10^6 m) over the IO (*left column*), WP (*middle column*) and CP (*right column*) regions. See the text for the definitions of the WWB measure. *Red* and *blue bars* denote the distributions of WWBs in observations and CAM4, respectively. *Green bars* show the ranges of ensemble spreads for the CAM4

of WWB measure over the equatorial Pacific indicates CAM4 is capable of reproducing the seasonal interaction between WWBs and the underlying surface.

The WWB occurrence and WWB measure indices also exhibit strong interannual variabilities. As shown in Table 1, the correlation coefficients of the annual mean WWB occurrence indices between the model ensemble mean and observations in the three target regions are statistically significant at a 95% confidence level (bottom panel), indicating that CAM4 is capable of capturing the interannual variability of WWB occurrence. However, there are three (one) ensemble members that show insignificant correlation coefficients for the IO (WP). The interannual variability of the WWB measure in all three regions is also significantly correlated with observations for all five ensemble members and the ensemble mean (Table 1).

3.3 Relation between WWBs and MJO

Previous studies indicated that WWBs prefer to occur at the convectively active phase of the MJO (Puy et al. 2015). In addition, strong MJOs tend to bear the local WWBs (Seiki and Takayabu 2007). Figure 5 shows the composite 20–100-day bandpass-filtered OLR and surface wind anomalies as a function of the MJO phases simulated by CAM4#1. The results from other four ensemble members are similar. Only the days with active MJO, i.e., the MJO index greater than 1.0, are used to make the composite. Following Wheeler and Hendon (2004), the MJO is decomposed into eight phases. As pointed out by Subramanian et al. (2011), CAM4 is capable of capturing the basic features of MJO, including the eastward propagation of the OLR anomalies and the prevailing surface westerlies under the negative OLR anomalies. However, the eastward propagation of the convection in the IO and WP regions is underestimated in model (Subramanian et al. 2011). In addition, the zonal fetch of the convection (depression) simulated in CAM4 is much broader than that in the observations (Li et al. 2016).

Table 1 Correlation coefficient of the yearly-mean WWB occurrence (before slash) and yearly-mean WWB measure (after slash) between CAM4 and observations

Model	IO	WP	CP
CAM4#1	0.27/0.47	0.38/0.39	0.53/0.80
CAM4#2	***0.22***/0.43	0.45/0.36	0.39/0.79
CAM4#3	0.36/0.45	***0.21***/0.30	0.56/0.85
CAM4#4	***0.23***/0.31	0.34/0.36	0.41/0.85
CAM4#5	***0.18***/0.32	0.39/0.58	0.61/0.84
Ensemble mean	0.34/0.47	0.48/0.46	0.62/0.84

Bold and italic texts indicate the correlation is insignificant at 95% confident level

Figure 6 shows the histograms of the percentage of days with WWBs as a function of the MJO phases. Note that Phase 'IA' indicates the days of WWBs when MJO is inactive (i.e., the MJO index is smaller than 1.0). In both observations and CAM4, there are about 30% WWBs occurring when MJO is inactive, suggesting that WWBs are not necessarily accompanied with the MJO (Vecchi 2000; Chiodi et al. 2014). However, in both observations and model simulations, more WWBs are found when MJO is at the convectively active phases (the phase with strong surface westerlies over the target regions), as noted in Seiki and Takayabu (2007). In order to examine whether the convectively active phase of the MJO can significantly influence the WWB occurrence, the significance of the percentage of the WWBs occurring in a given MJO phase is tested assuming a binomial distribution, which has a probability of $\frac{1-p}{8}$ (Vecchi 2000) where p denotes the percentage of WWBs occurring over a given region when MJO is inactive and the denominator of 8 is the number of MJO phases. As can be seen, the occurrence of observed WWBs over the IO region in Phase 5 is statistically significant, implying the strong impact from the MJO on WWBs over the IO region (Fig. 6a), while the percentage in Phase 4 and 6 are not significant, suggesting the weak influence of the MJO on the chance of seeing a WWB over the IO region (Chiodi et al. 2014). However, CAM4 does not show such a strong connection (Fig. 6d). Over the CP region, the impact of the MJO on the WWB occurrence is insignificant (Fig. 6c). For CAM4, the ensemble mean is also insignificant, although individual members suggest the significant influence of the simulated MJO in Phase 8 (Fig. 6f). Over the WP region, the significant modulation of MJO on WWB occurrence is well captured by model.

Figure 7 presents the percentage of the days with WWBs over the three regions, as a function of the normalized 20–100-day bandpass filtered OLR anomalies in observations and simulations. The histograms are binned to every 0.5 standard deviation for each region. The normalized OLR is used here to represent the magnitude of MJO in a given region. Note the latitude range of the OLR anomaly spans from 15°S to 15°N, the same latitude range used to calculate the MJO index. Because the days with extreme normalized OLR anomalies (smaller than −4 or greater than 4) are very sparse, only results obtained with at least 10 samples in bins are shown. In general, the percentage of days accompanied with the local WWBs increases when the normalized OLR anomalies become more negative in observations (red lines), indicating that strong MJO creates a favorable condition, though not sufficient, to influence the WWB occurrence (Seiki and Takayabu 2007). CAM4 generally captures such relationship over the three regions. When the normalized OLR anomalies are extreme strong (strong depression), the percentage of days with

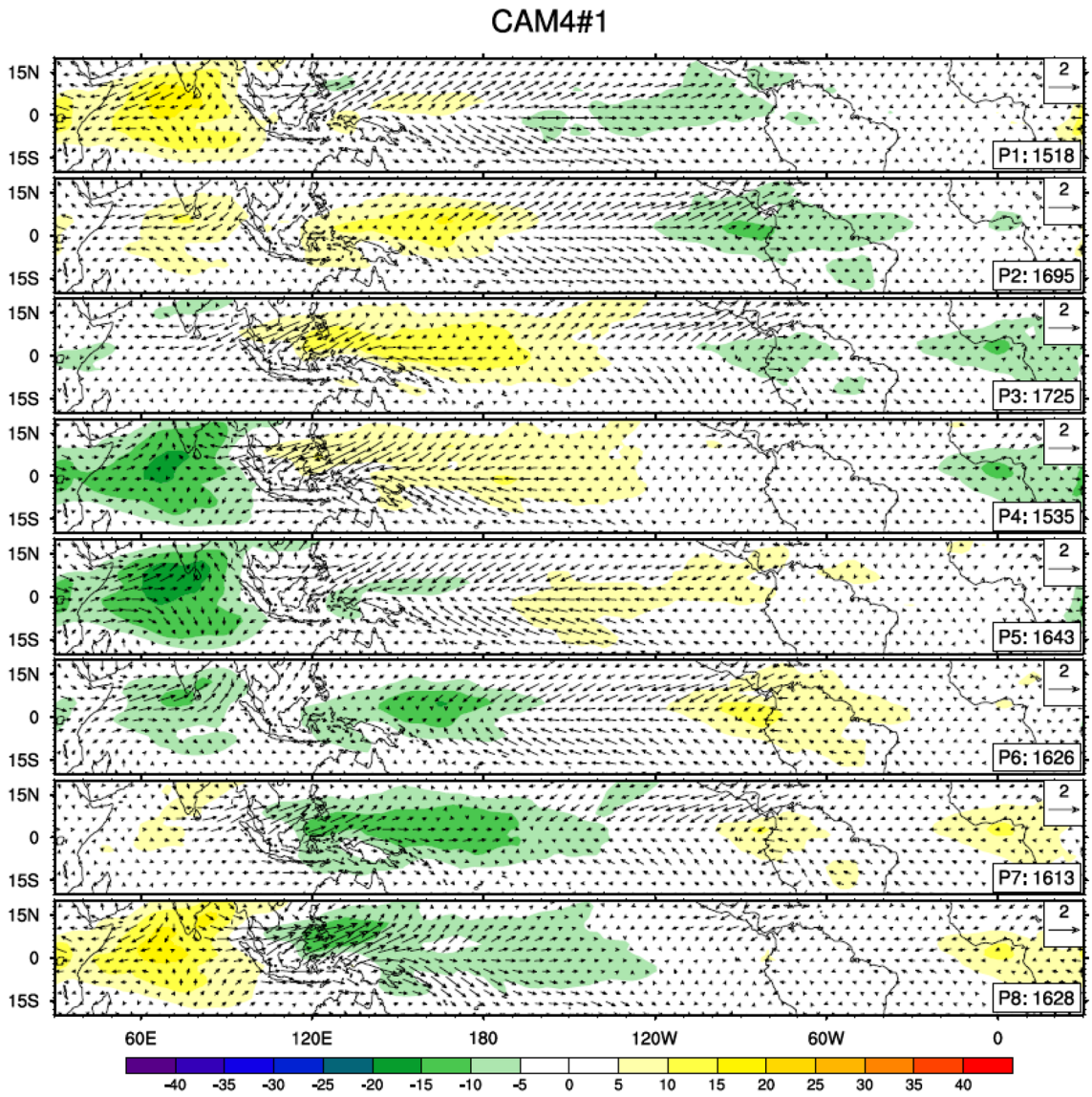

Fig. 5 Composite intraseasonal OLR (*color*, in Wm^{-2}) and surface wind anomalies (vectors) as a function of the MJO phases for CAM4#1. Number of days used to generate the composite for each phase is shown at the *bottom right* of each panel

the observed WWBs sharply increase in the CP region (Fig. 7c), suggesting that WWBs over the CP region are not necessarily accompanied with local deep convection. Detailed analysis indicates that those WWBs are closely associated with the surface westerly anomalies induced by the El Niño (not shown).

3.4 Relation between WWBs and ENSO

As shown in many studies, the occurrence and wind measure of the WWBs are significantly correlated with ENSO (e.g., Harrison and Vecchi 1997; Eisenman et al. 2005). Figure 8a–c shows the cross-correlation between the monthly-mean WWB occurrence in the three regions and the Niño 3.4 index. As stated in Seiki and Takayabu (2007), there is a significant negative correlation between the WWB occurrence in the IO region and ENSO in the observations, with a peak correlation of −0.18 when the ENSO lags WWBs by 1 month (Fig. 8a). This negative correlation is well captured by CAM4, indicating CAM4 prefers to generate WWBs in the IO region during La Niña year. For the WP region (Fig. 8b), the observed monthly mean WWB occurrence has a highest positive correlation of 0.22 when ENSO lags by 6 months, implying the WWBs prefer to occur before El Niño (Harrison and Vecchi 1997; Vecchi and Harrison 2000). CAM4 also shows a maximum positive correlation when ENSO lags by 6 months, although the lead-lag correlation curve

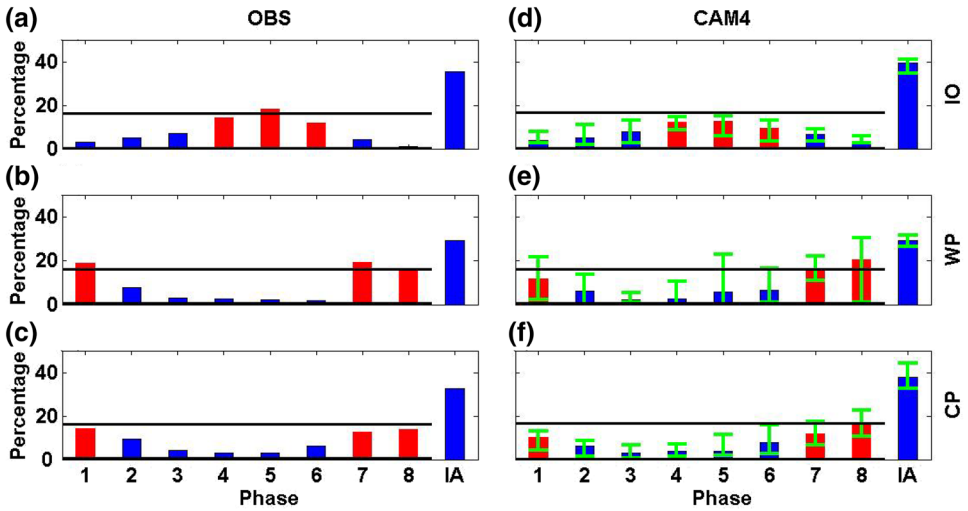

Fig. 6 The histograms of the percentage of WWBs occurring over the IO (*upper row*), WP (*middle row*) and CP (*lower row*) regions in observations (*left panel*) and CAM4 (*right panel*) as a function of the MJO Phase. Phase IA indicates that MJO is inactive. *Red bars* denote the convective active phase for each region. *Green bars* show the ranges of ensemble spreads. *Black lines* denote the 95% significant level of a binomial distribution. See text for details

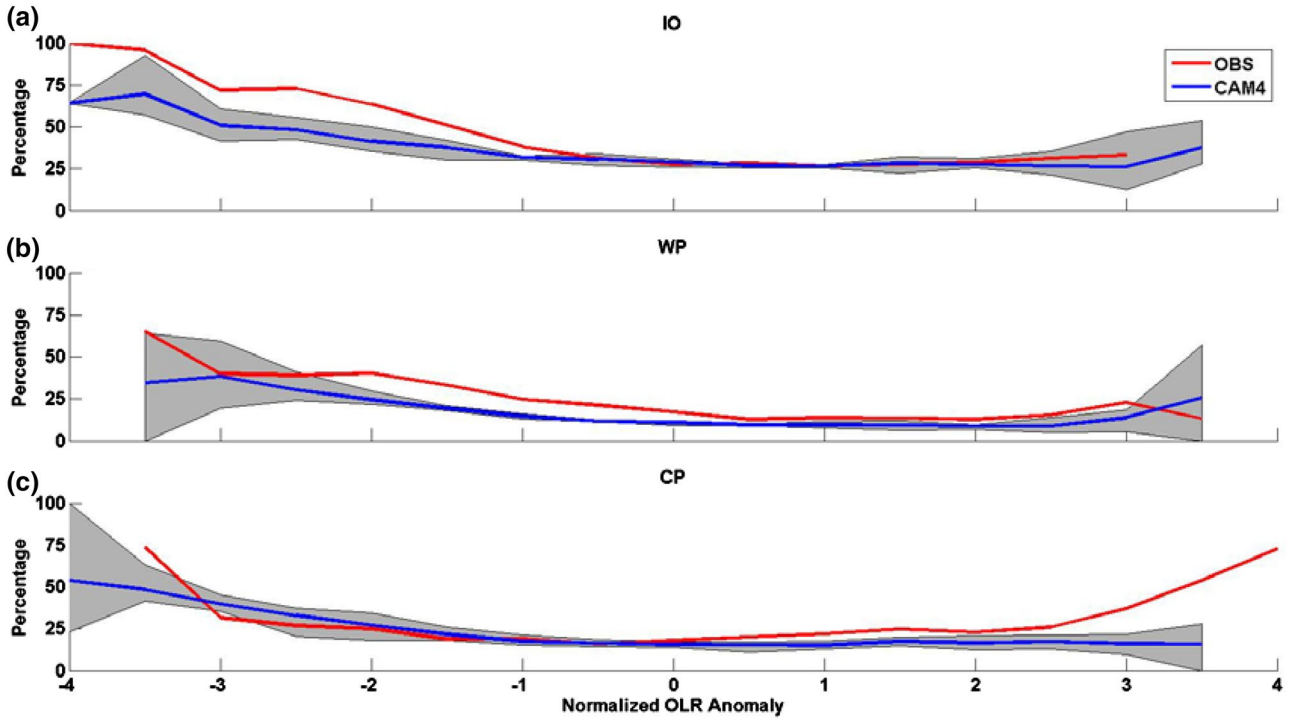

Fig. 7 The percentage of the days with WWBs over IO (*upper*), WP (*middle*) and CP (*lower*) region as a function of the normalized 20–100-day bandpass filtered OLR in observations (*red curve*) and the CAM4 (*blue curve*). *Grey shading* indicates the range of ensemble spreads. The histograms are binned to every 0.5 standard deviations for each region, and only bins with at least 10 samples are presented

is relatively flat. For the CP region (Fig. 8c), the WWB occurrence is almost in-phase with ENSO. The maximum correlation is 0.51 when ENSO lags by 1 month in observations. This feature is reproduced by CAM4. Figure 8d–f shows the cross-correlation between the monthly mean WWB measure and the Niño 3.4 index. The strong impact of ENSO on WWBs magnitude is well reproduced by CAM4.

Many studies indicated that the number of the equatorial Pacific WWBs during the El Niño years is much larger than the number during the La Niña years (Harrison and Vecchi 1997; Vecchi and Harrison 2000; Lian et al. 2014; Chen et al. 2015). Table 2 compares the ratio of the WWB occurrence during the El Niño and La Niña years in CAM4 and observations. As can be seen in Table 2, the occurrence of observed WWBs is larger during the La Niña years than

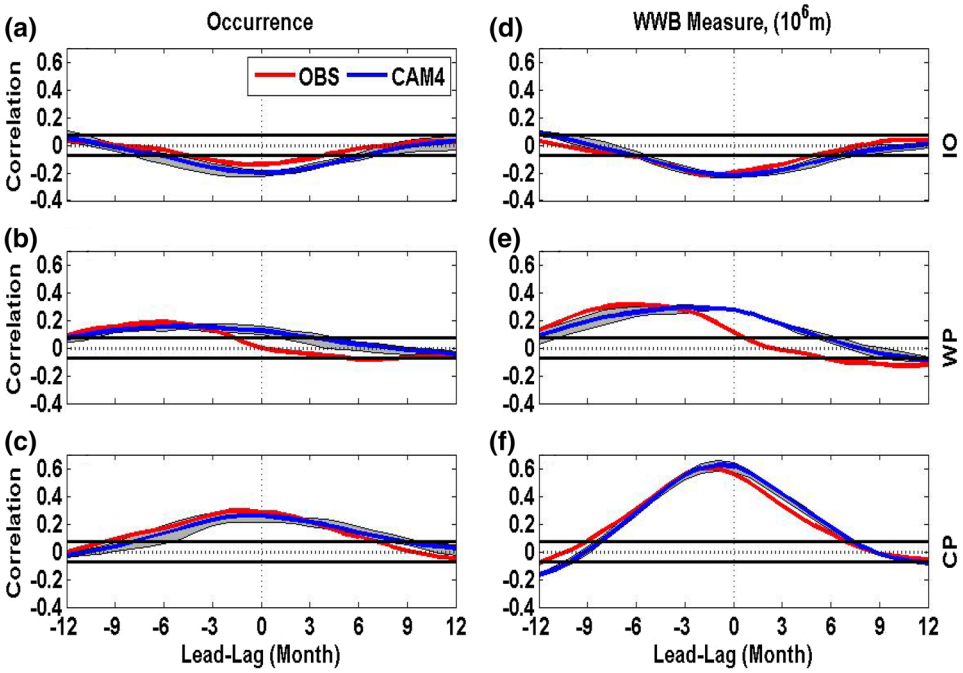

Fig. 8 Lead-lag correlation between the Niño 3.4 index and the monthly-mean WWB occurrence (*left panel*) and WWB measure (*right panel*, unit of 10^6 m) for the IO region (*upper*), WP region (*middle*), and CP region (*lower*) for observations (*red lines*) and CAM4 (*blue lines*). Negative lag means the WWB leads the Niño 3.4 index. *Black solid lines* indicate the 95% confident level. *Black dotted lines* denote zeros. *Grey shading* indicates the range of ensemble spreads

Table 2 Ratio of the averaged WWB occurrence during El Niño and La Niña year in observations and models

	IO	WP	CP
OBS	0.87	2.44	4.00
CAM4#1	0.57	4.71	7.75
CAM4#2	0.62	8.00	2.82
CAM4#3	0.62	2.73	8.20
CAM4#4	0.56	3.50	3.10
CAM4#5	0.46	4.67	7.00
Ensemble mean	0.56	4.72	5.77
CCSM4	0.39	5.69	19.56

Table 3 Regressive coefficient of the annual mean WWB occurrence (before slash) and WWB measure (after slash) against the Niño 3.4 (DJF) index in observations and models

	IO	WP	CP
OBS	−0.66/−1.96	0.83/5.23	1.38/11.75
CAM4#1	−0.85/−1.87	0.79/6.07	1.13/10.16
CAM4#2	−0.87/−1.53	0.70/7.34	1.03/12.12
CAM4#3	−0.93/−1.63	0.78/7.46	1.38/11.65
CAM4#4	−0.82/−2.08	0.70/6.49	0.72/11.12
CAM4#5	−1.28/***−1.03***	0.69/6.95	0.98/9.82
Ensemble mean	−0.95/−1.63	0.73/6.86	1.05/10.97
CCSM4	−1.32/−4.68	1.05/10.43	1.65/11.51

Bold and italic texts indicate the correlation is insignificant at 95% confident level

during the El Niño years in the IO region. Over the WP and CP region, as shown in previous studies, more WWBs are found during the El Niño years than the La Niña years. This difference is clearly reproduced by CAM4.

Table 3 lists the regression coefficient of the WWB occurrence (before slash) and WWB measure (after slash) against the Niño 3.4 (DJF) index. Both the annual mean WWB occurrence and WWB measure in the three regions are highly correlated with ENSO. In the IO region, the model indicates that the occurrence and wind measure of WWBs are negatively correlated with ENSO, whereas in the WP and CP regions their relations turn to positive. These findings are also consistent with the observations.

4 WWB simulations in CCSM4

4.1 General features

Figure 9 compares the longitudinal distribution of WWB occurrence and WWB measure in observations and CCSM4. Over the WP and CP regions, the longitude distribution of numbers and magnitudes of WWBs in each region are comparable with the observations. In the IO region, although the simulated WWB occurrence is comparable with observations, the strength of WWBs simulated in western IO is overestimated. The mean numbers of WWBs in the IO, WP, and CP regions are 4.44, 2.06, and 2.20 per year, respectively. As in the CAM4 experiments,

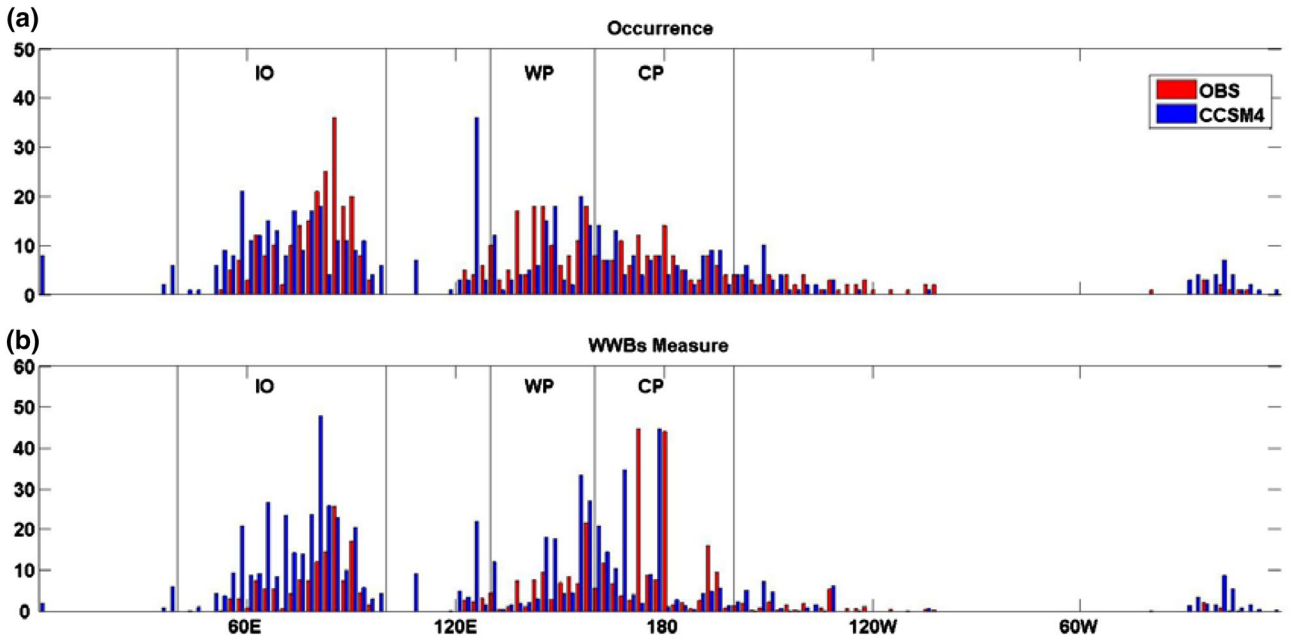

Fig. 9 Longitudinal distribution of the integrated WWB occurrence (**a**) and the annual mean WWB measure (**b**) in observations and CCSM4

the number of WWBs is underestimated in CCSM4. For the duration and zonal extension of WWBs, unlike what the CAM4 experiments, there are many simulated WWBs in the IO and WP regions with a long duration and a large zonal extension. In the CP region, the duration and zonal extension of WWBs are well simulated (not shown).

4.2 Seasonal and interannual variabilities of WWBs

The monthly distributions of WWB occurrence, days with WWBs and WWB measure in observations and CCSM4 simulations are compared in Fig. 10. Generally speaking, CCSM4 successfully reproduced the seasonal variabilities of those characteristics of WWBs, especially in the IO and WP regions. In the CP region, more and stronger WWBs are simulated around October, while the observed WWBs peak in December (Fig. 10f, i). Note that the simulated WWBs in the CP region are less occurred in boreal spring, and the strength of the WWBs in the CP region is severely underestimated in spring. The occurrence and strength of WWBs in the WP region are also underestimated in CCSM4 (Fig. 10e, h). Because the equatorial Pacific WWBs occurring in boreal spring is very important in triggering and maintaining the El Niño, such significant bias may lead to a poor preformation of ENSO in CCSM4.

The WWB occurrence and WWB measure indices also exhibit strong interannual variabilities in CCSM4. Figure 11 compares the evolution of WWBs in observations and CCSM4. In the equatorial Pacific, the eastern branch of the equatorial WWBs is basically confined to the west of 28.5 °C isotherm over the equatorial Pacific (Fig. 11a), implying the strong modulation of WWBs by the local SST, or in other words, by ENSO (McPhaden 1999; Yu et al. 2003). In addition, WWBs are found in the WP and CP (IO) regions during the El Niño (La Niña) years. The CCSM4 successfully captures the modulation of ENSO on the location of WWBs. However, more WWBs are simulated in the IO region, especially during the strong La Niña years. More discussions on the relation between WWBs and ENSO will be shown in Sect. 4.4.

4.3 Relation between WWBs and MJO

Figure 12 shows the histograms of the percentage of days with WWBs as a function of the MJO phases in observations and CCSM4 simulations. Note that the convective phase labels for observations have been adjusted, so that they are the same as in model; therefore, the labels of the convective phases (red bars) in observations are not the same as what are labeled in Fig. 6. Being consistent with the observations and CAM4 experiments, more WWBs are found during the MJO convective phases in CCSM4. In addition, the impact of the MJO convective phases on the WWB occurrence is insignificant in the IO region. In the WP region, the significant modulation to the WWB occurrence due to the MJO is reproduced. Although the impact of MJO on WWB occurrence in the CP region is insignificant in observations, it's shown in CCSM4 that MJO can significantly influence the number of WWBs in the CP region (Fig. 6f).

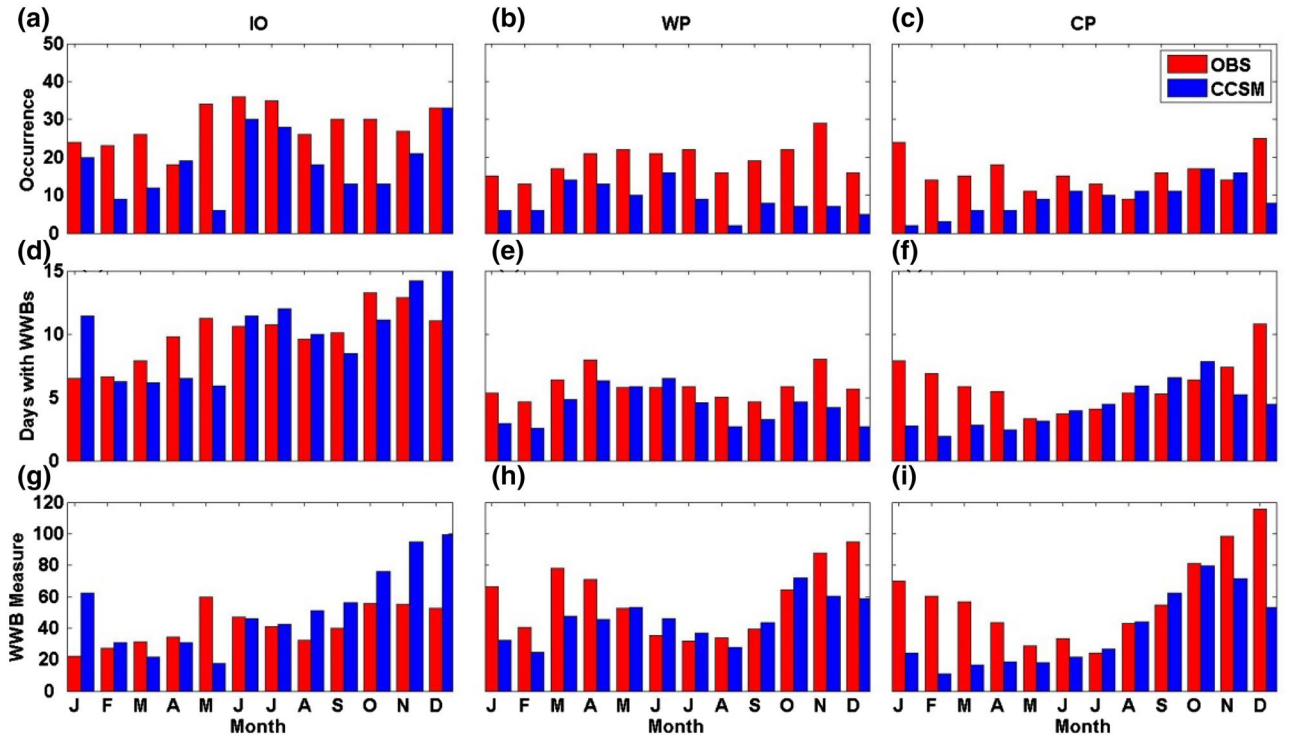

Fig. 10 Monthly distribution of the occurrence (*upper row*), number of days with WWBs (*middle row*), and WWB measure (*lower row*, unit of 10^6 m) over the IO (*left column*), WP (*middle column*) and CP (*right column*) regions. *Red* and *blue bars* denote the distributions of WWBs in observations and CCSM4, respectively

What is unexpected here is that the percentage of the days with WWBs over the three regions rapidly decreases when the MJO is extremely strong, as shown in Fig. 13. For example, in the case when the normalized 20–100-day bandpass filtered OLR anomalies are smaller than −3, which means strong deep convection occurs, only 25% days have WWBs in the IO region (Fig. 13a). In observations and the CAM4 ensembles, the percentages are 100 and 68%, respectively (Fig. 7). In the CP region, there are even no WWBs simulated in CCSM4 when the normalized OLR anomalies are less than −4. In observations and the CAM4 experiments, the percentage is more than 50%. Composite analysis indicates that when extreme negative OLR anomalies occur in these two regions, there are strong warming SST anomalies in the east of the center of negative OLR anomalies in CCSM4 (not shown). In addition, the center of warm SST anomalies is very close to the center of the negative OLR anomalies. The surface easterlies induced by the zonal SST gradient thus hamper the development of surface westerlies, and further the WWBs. In the CAM4 experiments, on the other hand, the zonal SST gradient on the east side of OLR anomaly center is much weaker. As a result, surface wind anomaly is dominated by the convection anomaly related to the MJO. The probability of WWBs is therefore higher. Further model experiments and analyses are needed to clarify whether the stronger zonal SST gradient in the east of the negative OLR center is a robust feature in CCSM4.

4.4 Relation between WWBs and ENSO

The cross-correlations between the monthly mean WWB occurrence in the three regions and the Niño 3.4 index are given in Fig. 14a–c. The WWB occurrence in the IO region has a significant negative correlation with ENSO. The largest correlation coefficient is −0.23 when ENSO lags WWBs by 2 months (Fig. 14a). In the WP and CP regions, the WWB occurrence is positively correlated with ENSO. The largest correlation occurs when WWBs lead ENSO by 3 months, indicating that WWBs also play a role in triggering the El Niño in the coupled model. The impact of WWBs on ENSO in the WP and CP regions, which is detected by the cross-correlations between the monthly mean WWB measure and the Niño 3.4 index, is stronger in the CCSM4 model than in the observations (Fig. 14d–f). However, the peak positive correlation in the WP region is more in-phase with ENSO in CCSM4 than in the observations, suggesting the role of WWBs in triggering the El Niño is underestimated in the coupled model. As in observations and CAM4, both the annual mean WWB occurrence and WWB measure in the three regions are highly correlated with ENSO (Table 3). In the

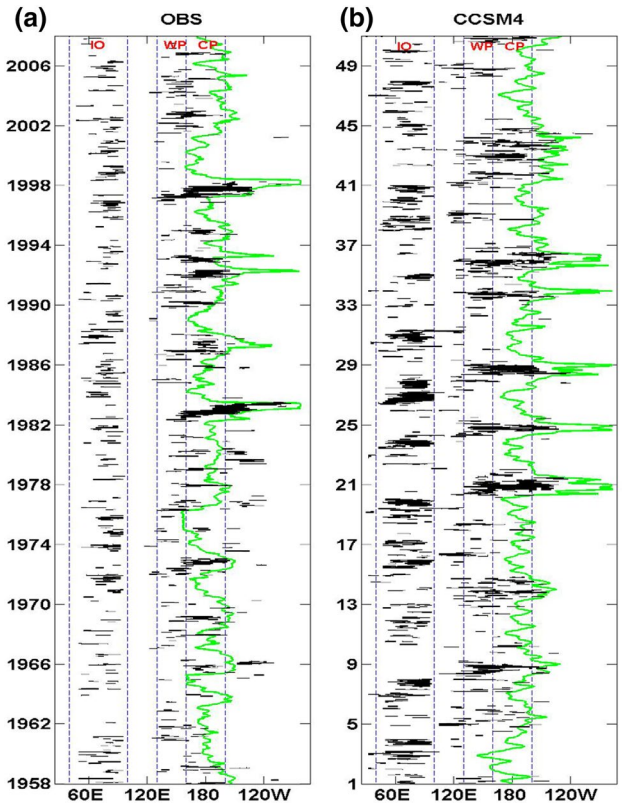

Fig. 11 Evolution of the 28.5 °C isotherm and WWBs along the equator in observations from 1958 to 2007 (**a**) and in CCSM4 from year 1 to year 50 (**b**)

IO region, the model indicates that the occurrence and wind measure of WWBs are negatively correlated with ENSO, whereas in the WP and CP regions their relations turn to positive.

As for the ratio of the WWB occurrence during the El Niño and La Niña year, however, large bias is found in the CCSM4 experiments compared to the CAM4 experiments, especially in the IO and CP regions. In the observations, the annual-mean WWB occurrences during the El Niño and La Niña year in the IO region are 5.22 and 6.00, respectively. In CCSM4, the annual-mean WWB occurrences are 2.22 and 5.75, respectively. WWBs occurred in the IO region during the El Niño is severely underestimated. The composite SSTs in CCSM4 show that the eastern tropical IO has a cold bias during the simulated El Niño years. Meanwhile, there is an easterly bias in the simulated zonal winds (not shown). In reality, the tropical IO region exhibits a basin-wide warming and weak surface wind anomalies in the El Niño years. In the CP region, the observed annual-mean WWB occurrences during the El Niño and La Niña years are 4.89 and 1.22, respectively. The simulated annual-mean WWB occurrences during the El Niño and La Niña year are 4.89 and 0.25, respectively. Because the MJO impact on WWB occurrence in the CP region is very weak in CCSM4 (Fig. 13c), WWB occurrence in the CP region is strongly dominated by ENSO, making few WWBs in the CP region in the La Niña years.

5 Origin of WWBs in CAM4

Previous studies found that the WWBs were always associated with strong deep convection near the center of WWBs (Seiki and Takayabu 2007). Figure 15 shows the surface wind anomalies and the 20–100-day bandpass-filtered OLR associated with the composite WWBs simulated in CAM4. Here, the composites are made from −10 to 10 days and for the relative longitude (RLO) from −60° to 60° from the

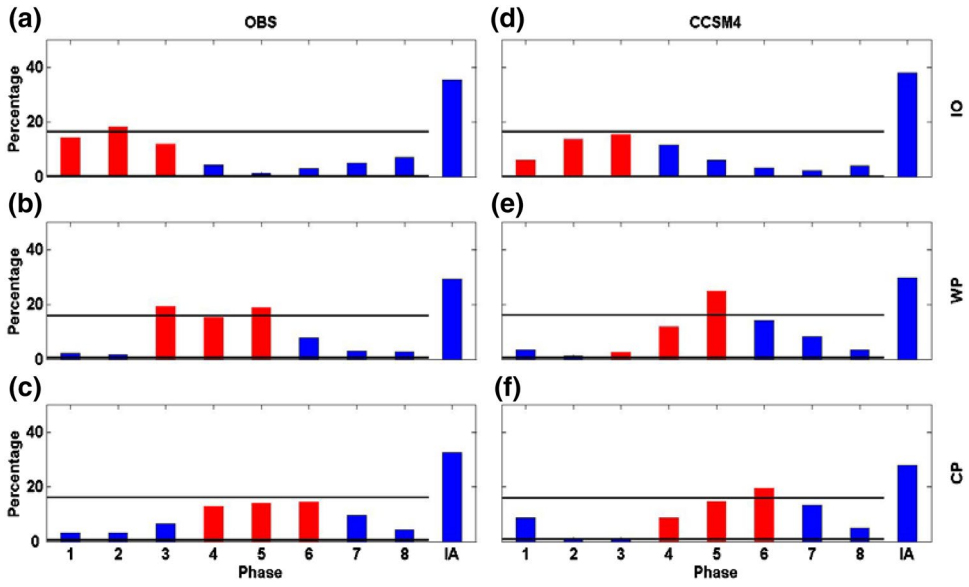

Fig. 12 The histograms of the percentage of WWBs occurring over the IO (*upper row*), WP (*middle row*) and CP (*lower row*) regions in observations (*left panel*) and CCSM4 (*right panel*) as a function of the MJO Phase. Phase IA indicates that MJO is inactive. *Red bars* denote the convective active phase for each region. *Black lines* denote the 95% significant level of a binomial distribution

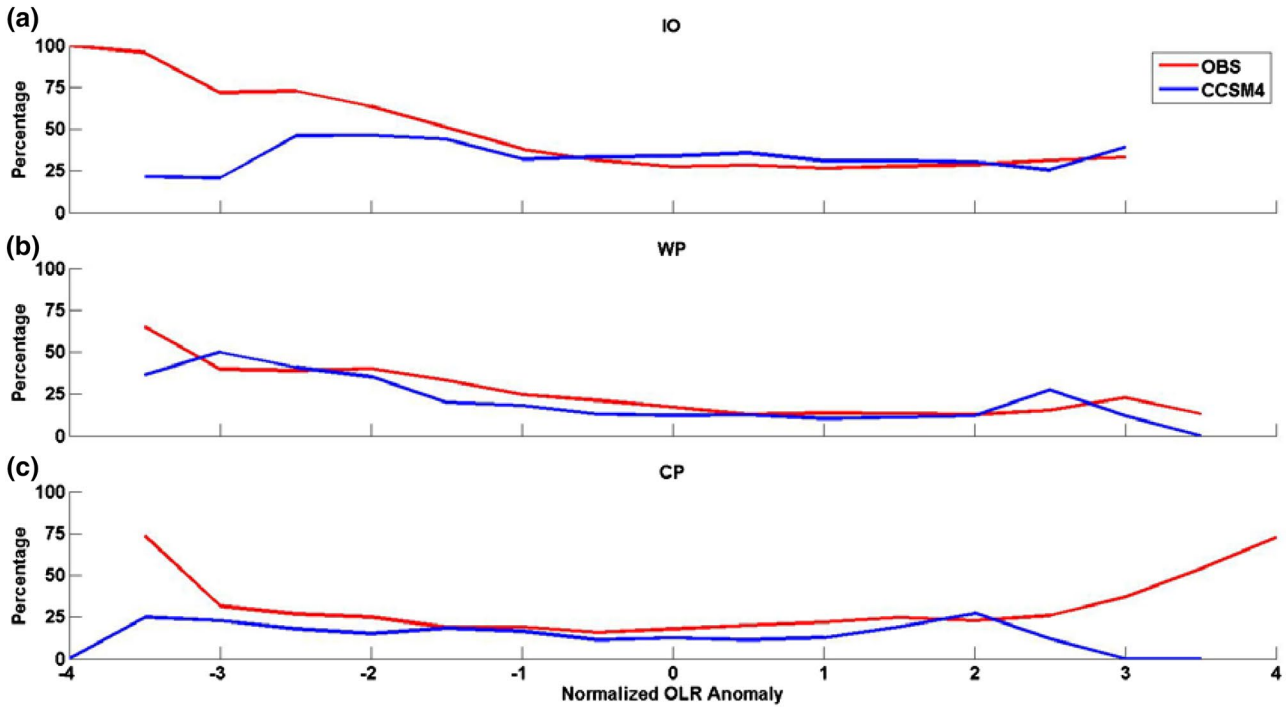

Fig. 13 The percentage of the days with WWBs over IO (*upper*), WP (*middle*) and CP (*lower*) region as a function of the normalized 20–100-day bandpass filtered OLR in observations (*red curve*) and the CCSM4 (*blue curve*). The histograms are binned to every 0.5 standard deviations for each region, and only bins with at least 10 samples are presented

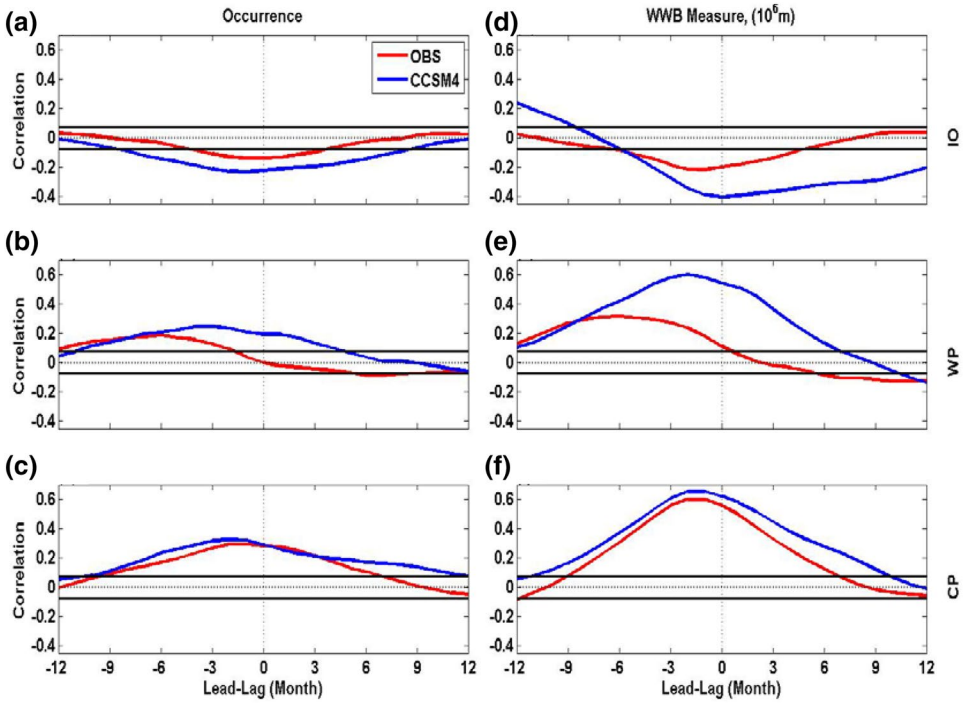

Fig. 14 Same as Fig. 8 but for the results from CCSM4

references. For example, 0° RLO on day 0 represents the longitude and the day at which WWBs reach the maximum zonal wind anomalies. Only the anomalous surface winds with a 95% confidence level are shown. The significance is tested using the one sample student's *t*-test. Over the IO and WP regions, the significant zonal wind anomalies

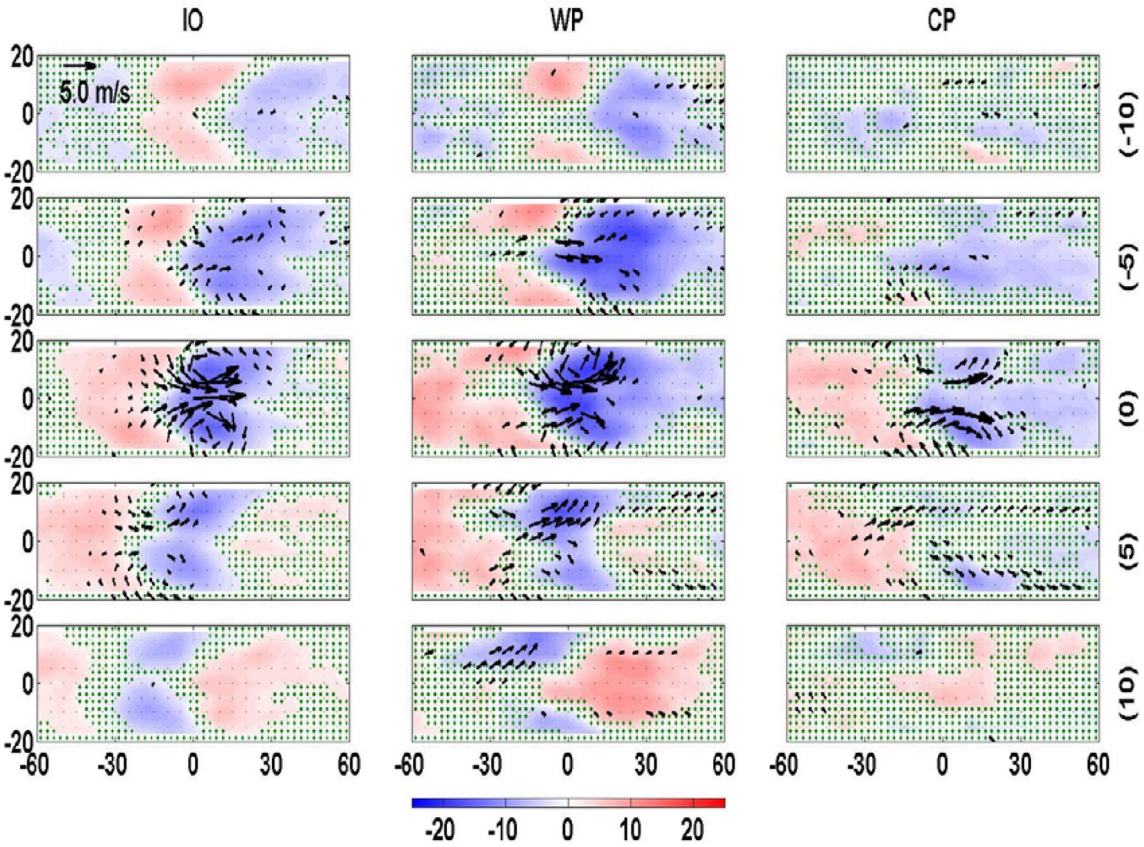

Fig. 15 Composite surface wind anomalies (vector, unit of m s^{-1}) and 20–100-day bandpassed OLR anomalies (*color*, unit of Wm^{-2}) during WWBs over the IO region (*left column*), WP region (*middle column*), and CP region (*right column*) in CAM4#1. *Number* in the *parenthesis* indicates the lag days from the reference day. Area with *green dots* is insignificant at a 95% confidence level. Only surface wind anomalies with a 95% confidence level are shown. The confidence level is estimated with the student's *t* test. The abscissa is relative longitude (RLO) and 0° RLO represents where WWBs attains its maximum zonal wind anomaly

increase on day −5 and decrease on day 5, whereas over the CP region the significant zonal wind anomalies last for a shorter duration from day 0 to day 5. Over all three regions, well organized negative OLR anomalies are found at the reference longitude, indicating WWBs are always accompanied by deep convection. In addition, weak positive OLR anomalies are found in the west of the deep convective centers. The negative OLR anomalies associated with WWBs in the CP region exhibit some distinct characteristics. Over the CP region, the negative OLR anomalies are mainly concentrated south to the equator, and is nearly stationary during the life time of WWBs. Over the IO and WP regions, on the other hand, the maximum negative OLR anomalies are symmetric to the equator, and those negative OLR anomalies move westward with speed of approximately 2.6 m s^{-1}, acting as equatorial Rossby waves (Puy et al. 2015).

The composite surface wind anomalies and 20–100-day bandpass-filtered OLR for the observations are shown in Fig. 16 for comparison. The observed negative intraseasonal OLR anomalies associated with WWBs are much weaker. Unlike CAM4, the negative OLR anomalies in the WP region are asymmetric to the equator and mainly allocated in the northern hemisphere. In addition, the westward movement of the observed negative OLR anomalies in the WP region is much slower than that of CAM4. In the IO region, the observed convective center even slightly moves eastward. Our findings suggest that although WWBs in the WP region are significantly associated with MJO (Figs. 6, 7), MJO is not the dominant factor in triggering local WWBs. It also indicates that CAM4 underestimates the association between WWBs and MJO in the IO and WP regions.

Despite those biases in simulating the spatial pattern of the surface wind anomalies and OLR anomalies associated with WWBs, the strong negative OLR anomalies are found in both observations and CAM4, indicating that the origin of WWBs in CAM4 may come from the deep convection. On the other hand, in CAM3, which is lack of WWBs (Lopez and Kirtman 2013; Lopez et al. 2013, and will be shown in Fig. 17a), the deep convection is neither

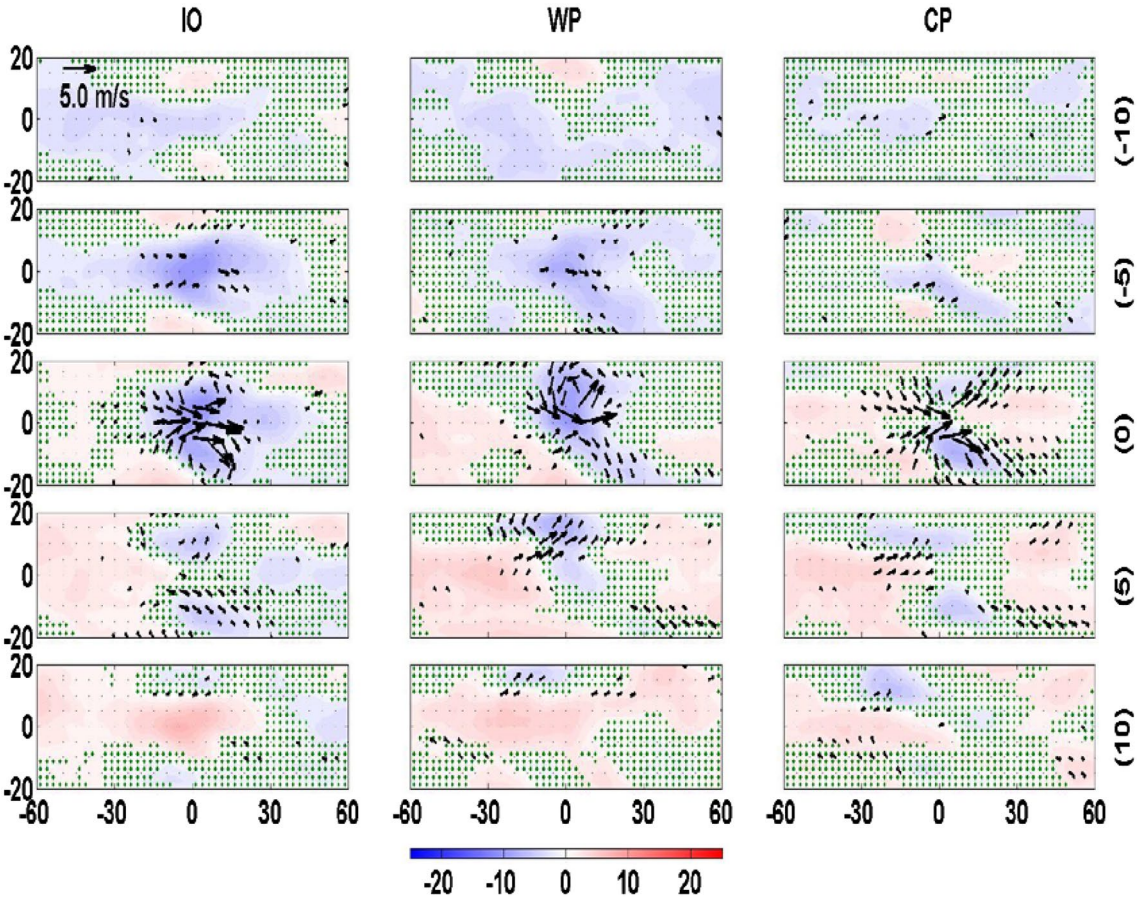

Fig. 16 Same as Fig. 15 but for observations

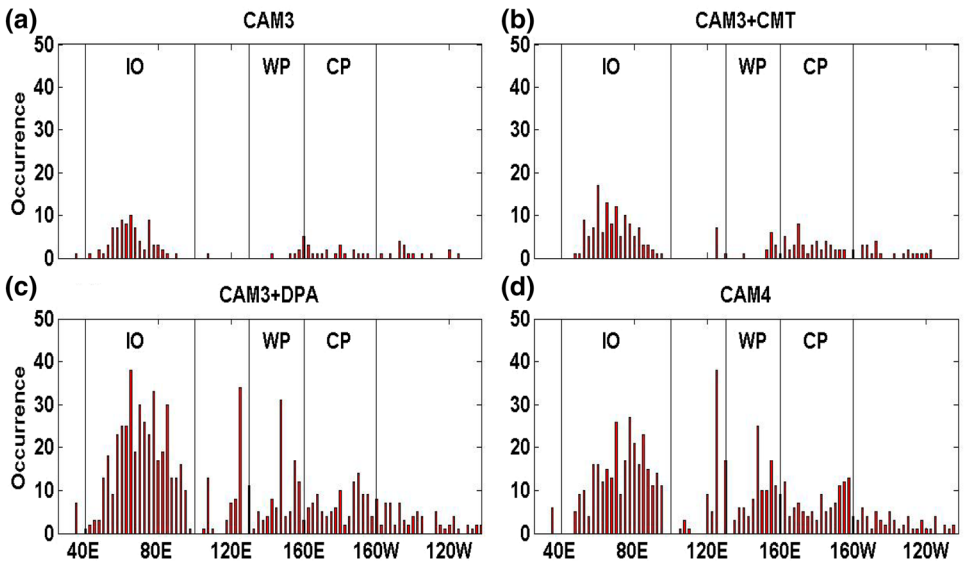

Fig. 17 Longitudinal distribution of the integrated WWB occurrence in CAM3 (**a**), CAM3 + CMT (**b**), CAM3 + DPA (**c**), and CAM4 (**d**)

found nor well organized, especially in the WP and CP regions (not shown).

As reported by Neale et al. (2013), compared to CAM3, CAM4 incorporates the convective momentum transports (CMT) and the dilute plume approximation (DPA) schemes which are favorable for increasing and strengthening the organized deep convection (Zhou et al. 2012). To test whether the deep convection plays a key role in inducing WWBs in CAM4, we design four model experiments with model physical modules set as CAM3, CAM3 + CMT, CAM3 + DPA and CAM4. The initial conditions used in these experiments are the same as those used in CAM4#1.

Figure 17 compares the longitudinal distribution of WWB occurrence found in CAM3, CAM3 + CMT, CAM3 + DPA and CAM4. As indicated in Lopez et al. (2013), very few WWBs are found over the equatorial Pacific in CAM3 (Fig. 17a). Although there are WWBs over the IO region, the number is much smaller than observations (Fig. 2a). The adoption of the CMT scheme increases the WWB occurrence, but the improvement is very weak (Fig. 17b). On the other hand, inclusion of the DPA scheme greatly increases the WWB occurrence (Fig. 17c), indicating that the DPA scheme is responsible for WWBs generation in CAM4 (Fig. 17d). The DPA scheme also plays a major role in improving the magnitude of WWBs, as indicated in Fig. 18c. However, over the CP region, the improvement of the annual mean WWB measure is mainly due to the CMT scheme (Fig. 18b, d).

Zhou et al. (2012) postulated that the DPA scheme can induce stronger intraseasonal variabilities by generating more available potential energy. Since the WWBs are accompanied with deep convection (Figs. 15, 16), the occurrence and the magnitude of WWBs thus increase when the DPA scheme is included. The CMT scheme represents the feedback of the unresolved properties to the background state, and mainly contributes to the improvement of the large-scale wind (Zhou et al. 2012). It thus plays a less important role in generating strong deep convection and WWBs. However, WWBs over the CP region are found to mainly occur during extreme El Niño years (Chen et al. 2015). The CMT scheme improves the surface westerly anomalies simulated during the El Niño years (not shown), thus prolongs the duration and zonal extension of WWBs, leading to the enhancement of the WWB measure over the CP region.

6 Conclusions and discussion

The WWBs simulations in CAM4 and CCSM4 are evaluated in this study. In both CAM4 and CCSM4 experiments, the longitude distribution of WWB occurrence is very close to the observations, with more WWBs occurred over the IO, WP, and CP regions. The durations of most simulated WWBs are less than 35 days, and the zonal extensions are in general less than 30° in longitude. These characteristics of the simulated WWBs are also confirmed by the NCEP/NCAR reanalysis. WWBs in the models exhibit strong seasonal and interannual variabilities. At the seasonal timescale, CAM4 has an acceptable performance in simulating the monthly distribution of WWB occurrence and strength. However, there is a significant bias in simulating the seasonality of the temporal peak of WWBs in the WP and CP regions, and a large model bias for the annual cycle of WWB measure. In CCSM4, the number of WWBs occurred in the equatorial Pacific and their strength is severely underestimated. At the interannual timescale, the simulated WWBs in both CAM4 and CCSM4 have a realistic reproduction over the three regions, especially over the WP and CP regions.

The relations between WWBs and MJO/ENSO are also explored. In reality, about 1/3 WWBs over the equatorial

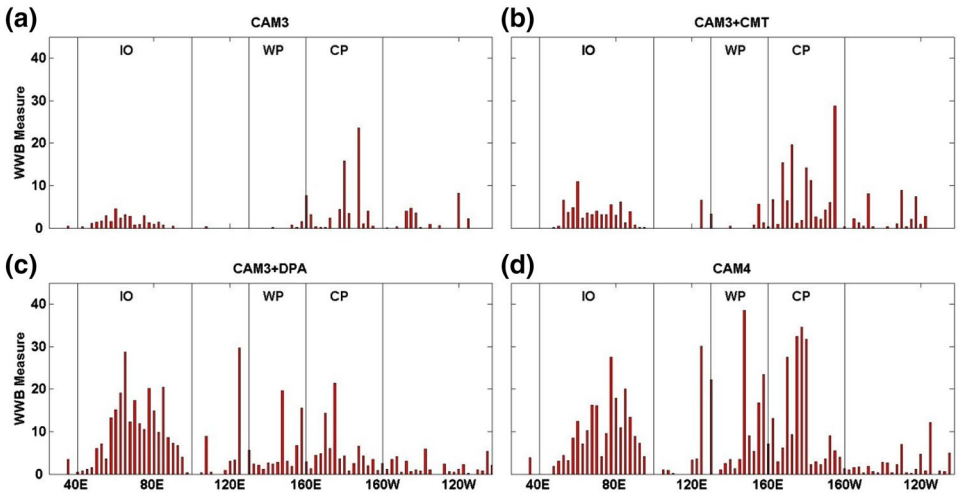

Fig. 18 Longitudinal distribution of the annual mean WWB measure (unit of 10^6m) in CAM3 (**a**), CAM3 + CMT (**b**), CAM3 + DPA (**c**), and CAM4 (**d**)

regions are found when MJO is inactive. For the WWBs occurring when the MJO is active, WWBs prefer to occur in the convectively active phases of the MJO. The preference of WWB occurrence in the convective phase of the MJO is also found in both CAM4 and CCSM4 experiments. In addition, significant influence of MJO on WWB occurrence over the WP region is well reproduced in models. For the effect of the strong MJO on WWB occurrence, the CAM4 experiments agree with the observations, i.e., WWBs prefer to occur with strong MJO. However, the strong modulation of extreme MJO to WWB occurrence is not found in CCSM4. This significant bias may be due to the bias in simulating the SST anomaly pattern associated with extreme MJO in the coupled model. Both the CAM4 and CCSM4 models successfully capture the robust relation between WWBs and ENSO, including the realistic out-of-phase (in-phase) relation between ENSO and WWBs in the IO (WP and CP) region, and the significant decrease (increase) of the occurrence and magnitude of WWBs over the IO region (WP and CP regions) with ENSO.

The origin of simulated WWBs is further explored in CAM4. In the IO and WP regions, strong and symmetric deep convections are found at the off-equatorial region when the WWBs reach the maximum, whereas in the CP region, the strongest deep convection is found south of the equator. By comparing the results from four different model experiments, the WWBs occurrence is found to be mainly due to the deep convection in the model. The inclusion of the DPA scheme, which is designed to enhance the organized intraseasonal variabilities, greatly increases the WWB occurrence in the model, and also plays a major role in improving the magnitude of the simulated WWBs. Less effect is found on WWB occurrence when the CMT scheme is included. However, the CMT scheme increases the magnitude of WWBs over the CP region via the enhancement of the surface westerlies during the strong El Niño years.

Despite the great model performance in simulating WWBs, there are still some significant differences between observations and model simulations. Among them, the severe underestimation of the number and strength of WWBs in the WP and CP regions in boreal spring may lead to a poor model performance in simulating ENSO. In addition, the simulated WWBs are too symmetric to the equator than the observations, and the convective center shows a westward movement as the equatorial Rossby waves. Other mechanisms, such as the cold surge and tropical cyclone which are also related to the WWBs may be missed in models (Keen 1982; Hartten 1996). Moreover, the westward propagation of simulated WWBs is too fast. Such fast movement may decrease the effects of WWBs on ENSO in models, since the forcing time for WWBs on the sea surface is reduced. The effect of cold surge and tropical cyclone on WWBs will be addressed in future studies.

Overall, our study illustrates that CAM4 and CCSM4 can reproduce the general spatiotemporal structure of the WWBs, and has an acceptable capability of reproducing the intraseasonal, seasonal, and interannual variabilities. Therefore, it is unnecessary to add the parameterization scheme for WWBs in CAM4. In addition, our findings validate the fact that, although containing the intrinsic stochastic atmospheric processes (Moore and Kleeman 1999; Fedorov 2002), the WWBs are greatly modulated by the SSTs (Yu et al. 2003; Tziperman and Yu 2007; Gebbie et al. 2007; Gebbie and Tziperman 2009). The bias in simulating WWBs in CCSM4, such as the lack of the equatorial Pacific WWBs in boreal spring and the weak modulation by strong MJO, is therefore due to the bias in the air-sea coupling, not in the atmospheric component.

The realist reproduction of the state-dependent relation between WWBs and ENSO in CAM4 provides us a potential and exceptional opportunity to improve ENSO forecasting. Current GCMs show poor prediction abilities of recent ENSO (Wang et al. 2010; Hu and Fedorov 2016). Menkes et al. (2014) showed that the lack of WWBs in boreal spring and summer is responsible for the weak El Niño in 2014. Lopez and Kirtman (2014) proposed that the spring prediction barrier of ENSO is partially caused by the lack of the WWBs in the forecast models. Improving the air-sea coupling may improve WWBs simulation in CCSM4, and may further improve the ENSO predictability in models. We will address these issues in a coming study.

Acknowledgements The NCEP reanalysis can be found in http://www.esrl.noaa.gov/psd/data. The CAM4 and CCSM4 code sources are from http://www.cesm.ucar.edu/models/ccsm4.0/cam. This work is supported by grants from the National Natural Science Foundation of China (41506025, 41690121, 41690120 and 41376034), the National Program on Global Change and Air–Sea Interaction (GASI-IPOVAI-02, GASI-IPOVAI-01-02, and GASI-IPOVAI-06) and the Zhejiang Provincial Natural Science Foundation of China (LQ15D060004).

References

Chen D, Lian T, Fu C, Cane M, Tang Y, Murtugudde R, Wu Q, Song X, Zhou L (2015) Strong influence of westerly wind bursts on El Niño diversity. Nat Geosci. doi:10.1038/ngeo2399

Chiodi AM, Harrison DE, Vecchi GA (2014) Subseasonal atmospheric variability and El Niño waveguide warming: observed effects of the Madden–Julian Oscillation and westerly wind events. J Clim 27:3619–3642

Collins WD, Rasch PJ, Boville BA, Hack JJ, McCaa JR, Williamson DL, Briegleb BP (2006) The formulation and atmospheric simulation of the Community Atmosphere Model version 3 (CAM3). J Clim 19:2144–2161

Eisenman I, Yu L, Tziperman E (2005) Westerly wind bursts: ENSO's tail rather than the dog. J Clim 18:5224–5238

Fedorov AV (2002) The response of the coupled tropical ocean–atmosphere to westerly wind bursts. Q J R Meteorol Soc 128:1–23.

Fedorov AV, Hu S, Lengaigne M, Guilyardi E (2014) The impact of westerly wind bursts and ocean initial state on the development, and diversity of El Niño events. Clim Dyn. doi:10.1007/s00382-014-2126-4

Gebbie G, Tziperman E (2009) Predictability of SST-modulated westerly wind bursts. J Clim 22:3894–3909

Gebbie G, Eisenman I, Wittenberg A, Tziperman E (2007) Modulation of westerly wind bursts by sea surface temperature: a semistochastic feedback for ENSO. J Atmos Sci 64:3281–3295

Gent PR, et al (2011) The Community Climate System Model version 4. J Clim 24:4973–4991

Harrison DE, Chiodi AM (2009) Pre- and post-1997/1998 westerly wind events and equatorial pacific cold tongue warming. J Clim 22:568–581

Harrison DE, Vecchi GA (1997) Westerly wind events in the tropical Pacific, 1986–95. J Clim 10:3131–3156

Hartten LM (1996) Synoptic settings of westerly wind bursts. J Geophys Res 101:16997–17019

Hu S, Fedorov AV (2016) Exceptionally strong easterly wind burst stalling El Niño of 2014. Proc Natl Acad Sci USA 113(8):2005–2010

Hu S, Fedorov AV, Lengaigne M, Guilyardi E (2014) The impact of westerly wind bursts on the diversity and predictability of El Niño events: an ocean energetics perspective. Geophys Res Lett 41:4654–4663. doi:10.1002/2014GL059573

Hunke EC, Lipscomb WH (2008) CICE: the Los Alamos sea ice model user's manual, version 4. Los Alamos Natl Lab Tech Rep LA-CC-06-012, pp 76.

Kalnay E et al (1996) The NCEP/NCAR 40-year reanalysis project. Bull Am Meteorol Soc 77:437–472

Keen RA (1982) The role of cross-equatorial tropical cyclone pairs in the southern oscillation. Mon Weather Rev 110:1405–1416

Kirtman BP, Straus DM, Min D, Schneider EK, Siqueira L (2009) Toward linking weather and climate in the interactive ensemble NCAR climate model. Geophys Res Lett 36:L13705

Lengaigne M, Boulanger J-P, Menkes C, Masson S, Madec G, Delecluse P (2002) Ocean response to the March 1997 westerly wind event. J Geophys Res 107:8015. doi:10.1029/2001JC000841

Lengaigne M, Boulanger J-P, Menkes C, Madec G, Delecluse P, Guilyardi E, Slingo JM (2003) The march 1997 westerly wind event and the onset of the 1997/98 El Niño: understanding the atmospheric response. J Clim 16:3330–3343

Lengaigne M, Boulanger J-P, Menkes C, Delecluse P, Slingo J (2004) Westerly wind events in the tropical Pacific and their influence on the coupled ocean-atmosphere system: a review. In: Earth climate: the ocean-atmosphere interaction, Geophys. Monogr. Ser, vol 147. AGU, Washington, D. C, pp 49–69

Li X, Tang Y, Zhou L, Chen D, Yao Z, Islam SU (2016) Assessment of Madden–Julian oscillation simulations with various configurations of CESM. Clim Dyn 47:2667–2690

Lian T, Chen D, Tang Y, Wu Q (2014) Effects of westerly wind bursts on El Niño: a new perspective. Geophys Res Lett 41:3522–3527. doi:10.1002/2014GL059989

Lian T, Chen D, Tang Y (2017) Genesis of the 2014–2016 El Niño events, Science China. Earth Sci. doi:10.1007/s11430-016-5315-5

Liess S, Bengtsson L, Arpe K (2004) The intraseasonal oscillation in ECHAM4 Part I: coupled to a comprehensive ocean model. Clim Dyn 22:653–669

Lopez H, Kirtman BP (2013) Westerly wind bursts and the diversity of ENSO in CCSM3 and CCSM4. Geophys Res Lett 40:4722–4727. doi:10.1002/grl.50913

Lopez H, Kirtman BP (2014) WWBs, ENSO predictability, the spring barrier and extreme events. J Geophys Res Atmos 119:10114–10138. doi:10.1002/2014JD021908.

Lopez H, Kirtman BP, Tziperman E, Gebbie G (2013) Impact of interactive westerly wind bursts on CCSM3. Dyn Atmos Oceans 59(1):24–51

Madden RA, Julian PR (1971) Detection of a 40–50 day oscillation in the zonal wind in the tropical Pacific. J Atmos Sci 28:702–708

McPhaden MJ (1999) Climate oscillations: Genesis and evolution of the 1997–98 El Niño. Science 283:950–954

McPhaden MJ, Freitag HP, Hayes SP, Taft BA, Chien Z, Wyrtki K (1988) The response of the equatorial Pacific Ocean to a westerly wind burst in may 1986. J Geophys Res 93(C9):10603

McPhaden M et al (2015) The curious case of the El Niño that never happened: a perspective from 40 years of progress in climate research and forecasting. BAMS doi:10.1175/BAMS-D-14-00089.1.

Menkes CE, Lengaigne M, Vialard J, Puy M, Marchesiello P, Cravatte S, Cambon G (2014) About the role of Westerly Wind Events in the possible development of an El Niño in 2014. Geophys Res Lett 41:6476–6483

Miyama T, Hasegawa T (2014) Impact of sea surface temperature on westerlies over the Western Pacific warm pool: case study of an event in 2001/02. SOLA 10:5–9. doi:10.2151/sola.2014-002

Moore AM, Kleeman R (1999) Stochastic forcing of ENSO by the intraseasonal oscillation. J Clim 12:1199–1220

Neale RB, Richter JH, Jochum M (2008) The impact of convection on ENSO: from a delayed oscillator to a series of events. J Clim 21:5904–5924. doi:10.1175/2008JCLI2244.1

Neale RB, Richter J, Park S, Lauritzen PH, Vavrus SJ, Rasch PJ, Zhang M (2013) The mean climate of the Community Atmosphere Model (CAM4) in forced SST and fully coupled experiments. J Clim 26:5150–5168. doi:10.1175/JCLI-D-12-00236.1.

Oleson KW et al (2008) Improvements to the Community Land Model and their impact on the hydrological cycle. J Geophys Res 113:G01021. doi:10.1029/2007JG000563

Puy M, Vialard J, Lengaigne M, Guilyardi E (2015) Modulation of equatorial Pacific westerly/easterly wind events by the Madden Julian oscillation and convectively coupled Rossby waves. Clim Dyn. doi:10.1007/s00382-015-2695-x.

Seiki A, Takayabu YN (2007) Westerly wind bursts and their relationship with intraseasonal variability and ENSO. Part I: statistics. Mon Weather Rev 135:3325–3345.

Seiki A, Takayabu YN, Yasuda T, Sato N, Takahashi C, Yoneyama K, Shirooka R (2011) Westerly wind bursts and their relationship with ENSO in CMIP3 models. J Geophys Res 116:D03303. doi:10.1029/2010JD015039

Smith RD et al (2010) The parallel ocean program (POP) reference manual. Los Alamos Natl Lab Tech Rep LAUR-10-01853, pp 140.

Subramanian AC, Jochum M, Miller AJ, Neale RB, Waliser DE (2011) The madden julian oscillation in CCSM4. J Clim 24:6261–6282. doi:10.1175/JCLI-D-11-00031.1

Tziperman E, Yu L (2007) Quantifying the dependence of westerly wind bursts on the large-scale tropical Pacific SST. J Clim 20:2760–2768

Vecchi GA (2000) Tropical Pacific sub-seasonal wind variability and El Niño, Ph.D. dissertation, Univ. of Wash., Seattle, pp 187

Vecchi GA, Harrison D (2000) Tropical Pacific sea surface temperature anomalies, El Niño, and equatorial westerly wind events. J Clim 13:1814–1830

Vecchi GA, Wittenberg AT, Rosati A (2006) Reassessing the role of stochastic forcing in the 1997–1998 El Niño. Geophys Res Lett 33:L01706. doi:10.1029/2005GL024738

Wang W, Chen M, Kumar A (2010) An assessment of the CFS real-time seasonal forecasts. Weather Forecast 25:950–969

Wheeler MC, Hendon HH (2004) An all-season real-time multivariate MJO index: development of an index for monitoring and prediction. Mon Weather Rev 132:1917–1932.

Xue Y, Kumar A (2016) Evolution of the 2015/16 El Niño and historical perspective since 1979. Sci China Earth Sci. doi:10.1007/s11430-016-0106-9.

Yu L, Weller RA, Liu TW (2003) Case analysis of a role of ENSO in regulating the generation of westerly wind bursts in the western equatorial Pacific. J Geophys Res 108:3128. doi:10.1029/2002JC001498

Zhou L, Neale R, Jochum M, Murtugudde R (2012) Improved Madden–Julian oscillations with improved physics: the impact of modified convection parameterizations. J Clim 25:1116–1136